Physica D 367 (2018) 11–18

Contents lists available at ScienceDirect

Physica D

journal homepage: www.elsevier.com/locate/physd

Turing patterns in parabolic systems of conservation laws and numerically observed stability of periodic waves

Blake Barker [a], Soyeun Jung [b,*], Kevin Zumbrun [c]

[a] Brigham Young University, Provo, UT 84602, United States
[b] Kongju National University, Republic of Korea
[c] Indiana University, Bloomington, IN 47405, United States

HIGHLIGHTS

- Conditions for Turing instability in conservation laws are derived.
- There exist no Turing-type instabilities in conservation laws for 2×2 systems.
- Stable periodic waves in conservation laws are numerically observed.

ARTICLE INFO

Article history:
Received 18 January 2017
Received in revised form 14 August 2017
Accepted 4 December 2017
Available online 7 December 2017
Communicated by K. Promislow

Keywords:
Turing instability
Conservation laws
Stable periodic waves

ABSTRACT

Turing patterns on unbounded domains have been widely studied in systems of reaction–diffusion equations. However, up to now, they have not been studied for systems of conservation laws. Here, we (i) derive conditions for Turing instability in conservation laws and (ii) use these conditions to find families of periodic solutions bifurcating from uniform states, numerically continuing these families into the large-amplitude regime. For the examples studied, numerical stability analysis suggests that stable periodic waves can emerge either from supercritical Turing bifurcations or, via secondary bifurcation as amplitude is increased, from subcritical Turing bifurcations. This answers in the affirmative a question of Oh–Zumbrun whether stable periodic solutions of conservation laws can occur. Determination of a full small-amplitude stability diagram – specifically, determination of rigorous Eckhaus-type stability conditions – remains an interesting open problem.

1. Introduction

The study of periodic solutions of conservation laws and their stability, initiated in [1,2] and continued in [3,4], etc., has led to a number of interesting developments, particularly in the related study of roll-waves in inclined shallow-water flow. For an account of these developments, see, e.g., [5] and references therein. However, in the original context of conservation laws, so far *no example of a stable periodic wave has been found.* Indeed, one of the primary results of [1,6] was that for the fundamental example of planar viscoelasticity, stable periodic waves do not exist, due to a special variational structure of this particular system; it was cited as a basic open problem whether stable periodic waves could arise for *any* system of conservation laws, either physically motivated: or artificially contrived.

In the more standard context of reaction–diffusion systems and classical pattern formation theory, by contrast, stable periodic solutions are abundant and well-understood, through the mechanism of *Turing instability*, or bifurcation of small-amplitude, approximately-constant period, periodic solutions from a uniform state. For such waves, stability is completely determined by an associated *Eckhaus stability diagram*, as derived formally in [7] and verified rigorously in [8–11], essentially by perturbation from constant-coefficient linearized behavior. By contrast, the small-amplitude waves investigated up to now (see Example 3.2) come through more complicated zero-wave number bifurcations in which period goes to infinity as amplitude goes to zero and the stability analysis is far from constant-coefficient (see, e.g., [12] in the successfully-analyzed case of shallow-water flow).

Our simple goal in this paper, therefore, is *to seek stable periodic waves via a conservation law analog of Turing instability.* In the first part, we find an analog of Turing instability, with which we are able to generate large numbers of examples of spatially periodic solutions of conservation laws. Next, we find an interesting dimensional restriction to systems of three or more

* Corresponding author.
E-mail addresses: blake@math.byu.edu (B. Barker), soyjung@kongju.ac.kr (S. Jung), kzumbrun@indiana.edu (K. Zumbrun).

https://doi.org/10.1016/j.physd.2017.12.003
0167-2789/

coordinates, explaining the absence of Turing instabilities for 2×2 systems considered previously. Finally, we perform a numerical existence/stability study for 3×3 example systems exhibiting Turing instability, answering in the affirmative the fundamental question posed in [1,6] whether there can exist stable spatially periodic solutions of systems of conservation laws, at least at the level of numerical approximation. These studies suggest that, for supercritical Turing bifurcation, stable waves can emerge through the small-amplitude limit and persist up to rather large amplitudes. For subcritical Turing bifurcations, all emerging waves are necessarily initially unstable, but appear in some cases to undergo secondary bifurcation to stability as amplitude is further increased.

The numerically observed stability of intermediate-amplitude waves we regard as conclusive. Delicacy of numerical approximation as amplitude goes to zero, however, prevents us from obtaining a detailed stability diagram near the Turing bifurcation or even from making definitive conclusions about stability in that regime. Rigorous spectral stability analysis for conservation laws in this regime, analogous to those of [8–11] in the reaction–diffusion case, we regard therefore as a very interesting open problem. The studies in [13,14] of reaction–diffusion equations with an associated conservation law may offer guidance in such an investigation.

2. Turing instability for conservation laws

We begin by defining a notion of Turing instability for systems of conservation laws

$$u_t + f(u;\varepsilon)_x = (D^\varepsilon u_x)_x, \tag{2.1}$$

$u \in \mathbb{R}^n$, where ε is a bifurcation parameter and D^ε for simplicity is taken constant. Linearizing (2.1) about a uniform state $u(x,t) \equiv u_0$ yields the family of constant-coefficient equations

$$u_t = L(\varepsilon)u := -A^\varepsilon u_x + D^\varepsilon u_{xx} \tag{2.2}$$

with dispersion relations $\lambda_j(\xi) \in \sigma(-i\xi A^\varepsilon - \xi^2 D^\varepsilon)$, $\xi \in \mathbb{R}$, where $\sigma(\cdot)$ here and elsewhere denotes spectrum of a matrix or linear operator. The state u_0 is spectrally (hence nonlinearly) stable if

$$\Re\sigma(-i\xi A^\varepsilon - \xi^2 D^\varepsilon) \le -\theta|\xi|^2, \quad \theta > 0, \tag{2.3}$$

for all $\xi \in \mathbb{R}$ [15].

Following the original philosophy applied by Turing [16] to reaction–diffusion systems, we seek a natural set of conditions guaranteeing *low- and high-frequency stability* – i.e., that (2.3) hold for $|\xi| \to 0, \infty$ – but allowing instability at finite frequencies $|\xi| \neq 0, \infty$. Should this be possible, then performing a homotopy in ε between stable and unstable states, we may expect generically to arrive at a special bifurcation point $\varepsilon = \varepsilon_*$, without loss of generality $\varepsilon_* = 0$, for which (2.3) holds uniformly away from special points $\xi = \pm\xi_*$, at which

$$\max_{\xi\neq 0} \Re\sigma(-i\xi A^{\varepsilon_*} - \xi^2 D^{\varepsilon_*}) = 0 \tag{2.4}$$

is achieved (note, by complex conjugate symmetry, that extrema appear in $\pm$ pairs) and for which (2.3) fails strictly as ε is further increased. We may then conclude, by standard bifurcation theory applied to the domain of periodic functions with period $X := 2\pi/\xi_*$ the appearance of nontrivial spatially periodic solutions with periods near X, similarly as in the reaction–diffusion case [8–11].

At $\xi = 0$, (2.3) yields that A^ε is hyperbolic, in the sense that it has real semisimple eigenvalues. Without loss of generality, therefore, take A^ε diagonal, with entries a_j, $j = 1, \dots, n$. In the simplest case that A^ε is *strictly hyperbolic,* in the sense that these a_j are distinct, we find by spectral perturbation expansion about $\xi = 0$ [15] that the corresponding eigenvalue expansions are

$$\lambda_j(\xi) = -ia_j\xi - D^\varepsilon_{jj}\xi^2 + O(\xi^3),$$

so that (2.3) ($\xi \ll 1$) is equivalent to the condition that D^ε *have positive diagonal entries* D^ε_{jj}. Similarly, by spectral expansion about $\xi = \infty$,

$$\sigma(-i\xi A^\varepsilon - \xi^2 D^\varepsilon) = -\xi^2\sigma(D^\varepsilon) + O(\xi),$$

so that (2.3)($\xi = \infty$) is equivalent to the condition that D^ε be unstable, i.e., *have eigenvalues with strictly positive real part*. Collecting, our hypotheses are $(\mathcal{C})$:

- A^ε is diagonal with distinct entries, and
- D^ε has positive diagonal entries and eigenvalues with strictly positive real part.

These are to be contrasted with Turing's conditions in the reaction–diffusion case $u_t = Du_{xx} + g(u)$ that D be symmetric positive and $A := dg(u)$ be symmetric negative definite [16].

2.1. Turing instability and Hopf bifurcation

Let (2.4) hold at a bifurcation point $\varepsilon = \varepsilon_*$ with $\lambda = \pm i\tau \in \sigma(-i\xi A^\varepsilon - \xi^2 D^\varepsilon)$ for $\xi = \pm\xi_*, \xi_* \neq 0$. Then, changing to the moving coordinate frame $x \to \tilde{x} := x - ct$, for $c := \tau/\xi_*$, or, equivalently, under the change of coordinates $A^\varepsilon \to \tilde{A}^\varepsilon := A^\varepsilon - cI$, we have $\lambda = 0 \in \sigma(-i\xi\tilde{A}^\varepsilon - \xi^2 D^\varepsilon)$ for $\xi = \pm\xi_*$, i.e., at a bifurcation point $\varepsilon = \varepsilon_*$, $\det(-i\xi\tilde{A}^\varepsilon - \xi^2 D^\varepsilon) = 0$ at $\xi = \xi_*$, or

$$\pm i\xi_* \in \sigma(D^{\varepsilon^{-1}}\tilde{A}^\varepsilon). \tag{2.5}$$

Condition (2.5) may be recognized as the condition for Hopf bifurcation of an equilibrium $u(x,t) \equiv$ constant of the traveling-wave ODE

$$D^\varepsilon u' = f(u;\varepsilon) - cu + q, \tag{2.6}$$

where q is a constant of integration, for which the linearized equation is $u' = D^{\varepsilon^{-1}}\tilde{A}^\varepsilon u$, $\tilde{A}^\varepsilon$ again diagonal. Thus, we recover by finite-dimensional bifurcation theory the previously-remarked appearance of nontrivial periodic solutions with period near $X = 2\pi/\xi_*$. We also obtain the alternative bifurcation criterion (2.5). *This simplifies the problem a great deal;* for one thing, we are now working with real matrices, as occur for symbols in the reaction–diffusion case, and not complex ones.

2.1.1. Dimensional count

From the usual Hopf bifurcation theorem for ODE, we find that for each fixed nearby q, c, there exists a one-parameter family of nontrivial periodic solutions bifurcating from the constant solution, generically parametrized nonsingularly by period X. Thus, fixing $q = 0$, we obtain a 2-*parameter family of periodic solutions, generically well-parametrized by c and X*.

2.2. Finding Turing instabilities

To find Turing instability, we may seek A^ε and D^ε satisfying $(\mathcal{C})$, $\varepsilon \in \mathbb{R}$ a bifurcation parameter, such that (2.4) is violated at $\varepsilon = 1$ (instability), but (2.3) is satisfied for all ξ at $\varepsilon = 0$ (stability), for example if $D^0 = \mathrm{Id}$. For, in this case, the conditions $(\mathcal{C})$ on A^ε, D^ε insure that at the largest value ε_* of ε for which (2.4) is satisfied, the maximum (2.4) is achieved at some $\xi = \xi_* \neq 0$, while for $\varepsilon > \varepsilon_*$ there must be strictly positive real part eigenvalues, again bounded uniformly away from zero.

As another approach, starting from the observation relating Turing instabilities and Hopf bifurcation, notice first that (2.4)

cannot occur when $D = I$ and A is diagonal with distinct entries, in which case the spectra of $(-i\xi A - \xi^2 D)$ are simply $\lambda_j(\xi) = -i\xi a_j - \xi^2$; nor can (2.5), since $\sigma(\tilde{A})$ is by assumption real. Thus, we suggest, first, finding examples $\check{A}$, $\check{D}$ satisfying (2.5) either analytically or by checking random matrices, then, setting up a homotopy $D^\varepsilon := \varepsilon\check{D} + (1-\varepsilon)I$ from the identity to $\check{D}$ (at this moment we assume $A^\varepsilon = \check{A}$). Since, as just observed, $\sigma(-i\xi\check{A} - \xi^2 D^\varepsilon)$ is stable for $\varepsilon = 0$, while for $\varepsilon = 1$ it is at most neutrally stable, having zero eigenvalues at $\xi = \pm\xi_* \neq 0$, we find that for some $\varepsilon_* \in (0, 1]$, $\sigma(-i\xi\check{A} - \xi^2 D^{\varepsilon_*})$ is exactly neutral, i.e., a *Turing instability*, with eigenvalues $\pm i\tau$ at $\xi = \pm\hat{\xi}_*$ (note: different from the original ξ_* in general!). As described above, this corresponds to a Hopf bifurcation in the traveling-wave ODE for speed $c_* := \tau/\hat{\xi}_*$, with limiting wave number $\hat{\xi}_*$ and period $X_* := 2\pi/\hat{\xi}_*$.

3. Negative results

We next describe situations in which Turing instability *cannot* occur, narrowing our search.

3.1. The 2×2 case

We have the following result for $n = 2$, strikingly different from the situation of the reaction–diffusion case.

Proposition 3.1. *Assuming* $(\mathcal{C})$, *there exist* no *Turing-type instabilities of* (2.1) *for* $n = 2$ *by showing that under the assumption* $(\mathcal{C})$ *there are no A and D satisfying* (2.5) *(for simplicity, we do not use a superscript "*ε_**").*

Proof. Take by assumption A diagonal. Since the entries of the matrix $D^{-1}A$ are real, appearance of a pure imaginary eigenvalue $i\tau$ implies the appearance also of its complex conjugate $-i\tau$, hence trace is zero and determinant is positive. By a scaling transformation $S = \begin{pmatrix}\alpha & 0\\ 0 & \beta\end{pmatrix}$ not affecting diagonal form of A, we may arrange therefore that $D^{-1}A = \begin{pmatrix}c & 1\\ -1 & -c\end{pmatrix} =: J$, for some $c^2 < 1$. Noting that $J^2 = (c^2-1)I$, we may solve to obtain $D = \frac{1}{c^2-1}AJ = \frac{1}{c^2-1}\begin{pmatrix}a_1 c & a_1\\ -a_2 & -a_2 c\end{pmatrix}$. The requirement that D have positive diagonal implies, with $c^2 < 1$, that $a_1 c < 0$ and $a_2 c > 0$, so that a_1 and a_2 have opposite sign. But, $\det D = (c^2-1)^{-2}a_1 a_2(1-c^2) > 0$ implies that a_1 and a_2 have the same sign, hence these two conditions cannot hold at once. □

Example 3.2. The viscoelasticity model $\tau_t - u_x = d_{11}\tau_{xx}$, $u_t + p(\tau)_x = d_{22}u_{xx}$ studied by Oh–Zumbrun [1] falls into the above framework, hence does not admit Turing instabilities. In fact, periodic waves arise in this model through Bogdanov–Takens bifurcation associated with splitting of two or more equilibria, a more complicated bifurcation far from constant-coefficient behavior.

3.2. Simultaneous symmetrizability

Another case in which Turing instabilities do not occur is when A and D are simultaneously symmetrizable, or, equivalently, can be converted by change of coordinates to be both symmetric (we again do not use a superscript "ε_*"). For, then, in the new coordinates, D, being symmetric positive definite, has a square root, and so $D^{-1}A$ is similar to the symmetric matrix $D^{1/2}D^{-1}AD^{-1/2} = D^{-1/2}AD^{-1/2}$, hence has *real eigenvalues*. More generally, it is easy to see that Turing instability does not occur for A symmetric and $H(D) := (1/2)(D + D^T) > 0$ (i.e., D with positive definite Hermitian part), since $D^{-1}Av = i\tau v$ would imply $0 = \Re i\tau\langle v, Av\rangle = -\tau^2\Re\langle v, Dv\rangle = -\tau^2\langle v, H(D)v\rangle < 0$, a contradiction. This recovers the well-known fact that existence of a viscosity-compatible convex entropy for the system (2.1) implies nonexistence of nonconstant stationary solutions, since existence of such an entropy implies the corresponding symmetry conditions on the linearized equations. Thus, taking A without loss of generality diagonal, we must specifically seek D *nonsymmetric*, $D + D^T$ *nonpositive* in order to find Turing instability.

3.3. Nonstrict hyperbolicity

Finally, we give a simple example showing that the condition of strict hyperbolicity of A^ε is necessary in $(\mathcal{C})$. Consider the matrices

$$A^\varepsilon = \begin{pmatrix}1 & 0 & 0\\ 0 & \varepsilon & 0\\ 0 & 0 & 1\end{pmatrix} \quad \text{and} \quad D^\varepsilon = \begin{pmatrix}1 & 0 & 2\\ 0 & 1 & 1\\ 1 & -2 & 1\end{pmatrix}. \tag{3.1}$$

Here, $\sigma(D) = \{1\}$; so $-i\xi A^\varepsilon - \xi^2 D^\varepsilon$ is stable for $|\xi| \to +\infty$. For $|\xi| \to 0$, we look at 2×2 blocks corresponding to the 1 and 3 entries of A^ε and D^ε,

$$\tilde{A} = \begin{pmatrix}1 & 0\\ 0 & 1\end{pmatrix} \quad \text{and} \quad \tilde{D} = \begin{pmatrix}1 & 2\\ 1 & 1\end{pmatrix}. \tag{3.2}$$

Then, the two eigenvalues of $-i\xi A^\varepsilon - \xi^2 D^\varepsilon$ close to $i\xi$ for $\xi \ll 1$ are by standard spectral perturbation theory $\lambda_j(\xi) = -i\xi - \xi^2\tilde{d}_j$, where $\tilde{d}_j$ are eigenvalues of $\tilde{D}$. We easily see that $\tilde{D}$ has two real eigenvalues with opposite sign because $det(\tilde{D}) = -1 < 0$. Thus, (2.3) is not satisfied for $|\xi| \to 0$.

Remark 3.3. Though example (3.1), failing $(\mathcal{C})$, does not itself yield Turing instability, it is quite useful in finding nearby systems that do. For, note perturbation in ε generates matrices $D^{-1}A$ with nonstable eigenvalues despite $A > 0$. Perturbing first ε to obtain instability, then A still more slightly to recover strict hyperbolicity, we thus obtain an example satisfying $(\mathcal{C})$ with unstable $D^{-1}A$, which yields a Turing bifurcation upon homotopy $D \to I$. We in fact used this method to generate the examples of Section 5. (We have generated other examples in other ways, that were not reported here; all exhibited similar behavior, however.)

4. Spectral and nonlinear stability

Before describing our numerical investigations, we briefly recall the abstract stability framework developed in [1,4,5], etc., relevant to stability of the nontrivial periodic waves bifurcating from a constant solution at Turing instability. First, recall [4,5] that, under the condition of transversality of the associated periodic orbit of the traveling-wave ODE (guaranteed in this case by the Hopf bifurcation scenario, for sufficiently small-amplitude waves), nonlinear stability with respect to localized perturbations of the periodic wave considered as a solution on the whole line is determined (up to mild nondegeneracy conditions) by conditions of *diffusive spectral stability*, as we now describe.

For given a periodic wave $\bar{u}$ with period X, the generic situation [3,17] is that up to translation the set of X-periodic solutions in the vicinity $\bar{u}$ forms a smooth $(n+1)$ dimensional manifold (the constant of integration $q \in \mathbb{R}^n$ in the traveling wave ODE (2.6) and the wave speed $c \in \mathbb{R}$). By Floquet theory, the $L^2(\mathbb{R})$ spectrum of the linearized operator L about $\bar{u}$ is entirely essential spectrum, corresponding to values $\lambda \in \mathbb{C}$ for which there exist generalized eigenfunction solutions $v(x) = e^{i\xi x}w(x)$, $\xi \in \mathbb{R}$, of the associated eigenvalue equation $(L - \lambda)v = 0$ with w periodic, period X. The dissipative stability conditions are that this spectrum have real part $\leq -\eta\xi^2$, $\eta > 0$, for all $\xi \in \mathbb{R}$, and strictly negative for $(\xi, \lambda) \neq (0, 0)$. In particular, for $\xi = 0$, $L\bar{u}' = 0$ and $\bar{u}$ is a

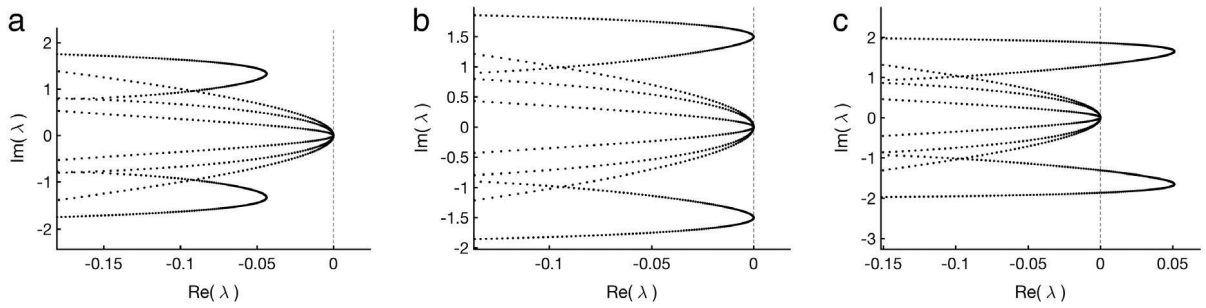

Fig. 1. Plot with dots of a sampling of the spectrum of the constant solution, $-i\xi A - \xi^2 D$, with (a) $\varepsilon = -0.2$, (b) $\varepsilon = 0$, (c) $\varepsilon = 0.2$. The dashed vertical line marks the imaginary axis.

periodic wave with period X implies that an eigenvalue $\lambda = 0$ has the multiplicity $(n+1)$.

For transversal orbits with ε bounded away from ε_*, the spectra near $(\xi, \lambda) = (0, 0)$ consists of the union of $(n+1)$ smooth spectral curves

$$\lambda_j(\xi) = -ia_j\xi + o(\xi)$$

through the origin $\lambda = 0$ for sufficiently small $|\xi|$. This was established in [17] using direct Evans function calculations and also proved in [18] based on direct spectral perturbation expansion. Moreover, under the nondegeneracy condition that a_j be distinct, this bifurcation is analytic in ξ, admitting second-order expansions

$$\lambda_j(\xi) = -ia_j\xi - b_j\xi^2 + O(\xi^3), \quad j = 1, \dots, n+1. \tag{4.1}$$

"Sideband", or low-frequency stability, is defined as $\Im a_j = 0$, $\Re b_j > 0$, i.e. stability to second order in ξ for $\xi \neq 0$. "Diffusive stability" may then be expressed as sideband stability plus the property that all spectra other than the curves described in (4.1) have real part strictly $\leq -\eta$ for some uniform $\eta > 0$. See [4,18] for more complete discussion from a general point of view.

In the case of Turing instability, choosing the period X_* such that the wave-numbers $\pm\xi_*$ at $\varepsilon = \varepsilon_*$ are equal to zero modulo $2\pi/X_*$, we find by direct Fourier transform calculation that the constant solution at $\varepsilon = \varepsilon_*$ has low-frequency spectrum consisting of $(n+2)$ *spectral curves passing through the origin,* with all other spectra satisfying $\Re\lambda \leq -\eta < 0$ for some $\eta > 0$. The spectra of the bifurcating periodic waves perturbs smoothly from these values as ε is increased, hence high-frequency diffusive stability is guaranteed. However, low-frequency stability is now determined by a possibly complicated bifurcation of $(n+2)$ spectral curves involving the $(n+1)$ curves (4.1) passing through the origin plus an additional curve originating from the constant limit passing close to but not through the origin. These curves are clearly visible in the numerically approximated spectra displayed below in Section 5 for example systems with $n = 3$: namely, 4 curves (4.1) passing through the origin, with a 5th (initially) neutral spectral curve passing near the origin, with all 5 of these passing through the origin at the bifurcation point $\varepsilon = \varepsilon_*$.

5. Numerical investigations

Guided by the results of Sections 2, 3, and 4, we now perform the main work of the paper, carrying out numerical existence and stability investigations for periodic solutions of systems of conservation laws arising through Turing bifurcation from the uniform state in dimension $n = 3$. Numerics are carried out using the MATLAB-based package STABLAB developed for this purpose [19]. We first briefly summarize our numerical observations.

5.1. A brief summary of results

In Section 5.2, by considering systems of conservation laws with a quadratic nonlinearity, we obtain stable periodic waves bifurcating from the Turing instability and moreover they exist through a supercritical Hopf bifurcation. In order to investigate both super and subcritical Hopf bifurcation, we consider systems of conservation laws with a cubic nonlinearity in Section 5.3. Indeed, in this case, we show there are stable periodic waves through both super and subcritical Hopf bifurcation by simply changing the sign of the nonlinearity, while it does not happened in the case of quadratic nonlinearity. However, the stable periodic waves we found from the cubic nonlinearity are not bifurcating from the Turing instability, but secondary bifurcation to stability as amplitude of waves is further increased.

5.2. Quadratic nonlinearity

We first consider the system

$$u_t + A^\varepsilon u_x + N(u)_x = Du_{xx}, \tag{5.1}$$

with

$$A^\varepsilon := \begin{pmatrix} 1 & 0 & 0 \\ 0 & a_{22}^0 + \varepsilon & 0 \\ 0 & 0 & 3 \end{pmatrix}, \quad D := \begin{pmatrix} 1 & 0 & 2 \\ 0 & 1 & 1 \\ 1 & -2 & 1 \end{pmatrix}, \quad \text{and}$$
$$N(u) := \beta \begin{pmatrix} u_1^2 \\ 0 \\ 0 \end{pmatrix}, \tag{5.2}$$

where $a_{22}^0 = 2.605173614560316$. Here, ε is a bifurcation parameter that we will vary and $u \equiv 0$ is a constant solution of (5.1). By linearization of (5.1) about $u = 0$, we have

$$u_t + A^\varepsilon u_x = Du_{xx}. \tag{5.3}$$

We first check Turing-type instability conditions for $u \equiv 0$ in (5.3). Notice that A^ε is strictly hyperbolic and D has positive diagonal entries with $\sigma(D) = \{1\}$, which means that $-i\xi A^\varepsilon - \xi^2 D$ is stable near $\xi = 0$ or $\xi = \pm\infty$. We examine numerically stability of $u \equiv 0$ as ε changes. In Fig. 1, we plot the spectrum of $-i\xi A^\varepsilon - \xi^2 D$ with $\varepsilon = -0.2$, $\varepsilon = 0$, and $\varepsilon = 0.2$. It is seen that the constant solution $u \equiv 0$ is stable for $\varepsilon < 0$ and unstable for $\varepsilon > 0$. Thus, Turing instability occurs at $\varepsilon = 0$, that is, (2.4) is satisfied with $\pm i\tau \in \sigma(-i\xi A^0 - \xi^2 D)$ for $\tau \approx 1.5$ and $\xi_* \approx \pm 1.16$. As we observed in the previous section, $\pm i\xi_*$ are eigenvalues of $D^{-1}(A^0 - c_* I)$ for $c_* = \frac{\tau}{\xi_*} \approx 1.30$. So the condition for Hopf bifurcation of a constant solution $u \equiv 0$ of the profile equation

$$-cu + A^\varepsilon u + N(u) = Du' + q \tag{5.4}$$

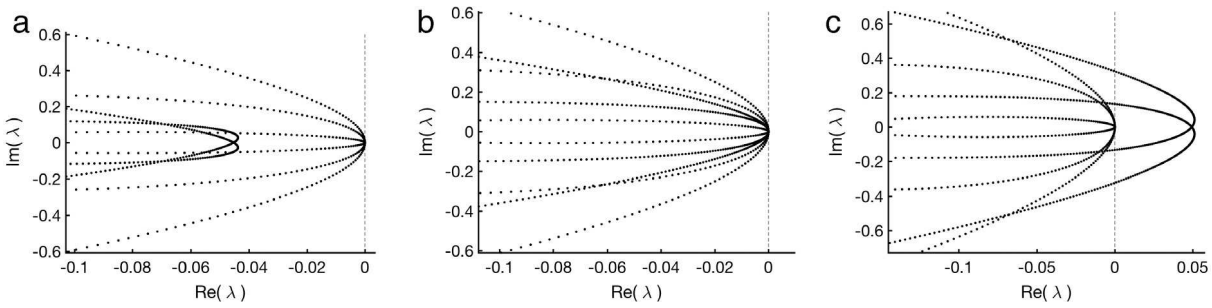

Fig. 2. Plot with dots of a sampling of the spectrum of the constant solution, $-i\xi(A - c_*I) - \xi^2 D$, with (a) $\varepsilon = -0.2$, (b) $\varepsilon = 0$, (c) $\varepsilon = 0.2$ and $c = c_* \approx 1.30$. The dashed vertical line marks the imaginary axis.

is satisfied at the bifurcating point $\varepsilon = 0$ and $c = c_*$. Here $q \in \mathbb{R}^3$ is an integration constant and we fix $q = 0$ from now on. In Fig. 2, we plot the spectrum of $-i\xi(A^\varepsilon - c_*I) - \xi^2 D$ for the same ε as in Fig. 1, showing how this moves the neutral spectrum from $\lambda = \pm i\tau$ to $\lambda = 0$.

The Hopf bifurcation leads to periodic profiles bifurcating from the uniform state $u \equiv 0$. In order to solve for these profiles, we let ε be a free variable and vary the period X and wave speed c, approximating associated solutions using the periodic profile solver built into STABLAB, which uses MATLAB's Newton-based boundary-value problem solver bvp5c. In addition to periodic boundary conditions, the profile solver specifies a phase condition $w \cdot f(y(0)) = 0$ where $y'(x) = f(y(x))$ is the profile ODE ((2.6) in the present case) and w is a random vector. Unless w is a degenerate choice, $w \cdot \dot{y}(t) = 0$ for some t by periodicity of y and Rolle's Theorem, so this phase condition chooses a solution (at least locally) uniquely. To numerically solve the profile equation with a quadratic nonlinearity, we first obtain a solution by using as an initial guess $u(x) = \sqrt{\varepsilon}\Re(e^{2\pi i x}v)/10$, where v is the real part of an eigenvector, whose corresponding eigenvalue has non-zero imaginary part, of the profile Jacobian evaluated at the fixed point $(0, 0, 0)^T$. That is, we start with an initial guess consisting of a strategically scaled periodic solution of the linearized equations at the bifurcation point $\varepsilon = 0$. Once we have a profile solution via this guess, we use continuation to solve for other profiles with nearby period X and speed c, obtaining thereby a full 2-parameter family of approximate solutions parametrized by (c, X), as described in Section 2.1.1.

In Fig. 3(a) and (b), we plot the stability bifurcation diagram in the coordinates of shifted wave speed $c^0 = c - c_*$ and period X. The bifurcation diagram shows that there is a family of stable waves bifurcating from the Turing bifurcation. There is a small region of instability occurring from a "parabolic" instability, or change in curvature of a neutral spectral curve through the origin, which separates the region of stability near the Turing bifurcation point and the larger stability region. Fig. 3(d)–(f) demonstrate the onset of this type of instability as seen in the spectrum of the bifurcating periodic waves. In Fig. 3(c), we see that the spectrum of the background constant solution becomes unstable as ε increases, so that the periodic profile shown in Fig. 3(g) comes into existence through a supercritical Hopf bifurcation. Finally, in Fig. 3(g), we plot the periodic profile for $\beta = -10$, $\varepsilon = 2.82e-3$, $c = c_* + 4.06e-3$, $X = 5.44$.

We note that, as described in Section 4, there are generically 4 neutral spectral curves passing through the origin. This is clearly visible in Fig. 3(d)–(f). However, as seen in Fig. 2(b), the constant solution has 5 spectral curves passing through the origin at the bifurcation point and the spectra of bifurcating periodic waves perturbs from these 5 curves. So, at the bifurcation point, there is a 5th neutral curve passing through the origin, which remains nearby for values of ε nearby ε_*. It explains why the spectrum of stable periodic waves bifurcating from Turing bifurcation in Fig. 3(d) has an additional 5th curve which is very close to the origin but not through the origin. Stability of small-amplitude waves is determined by behavior of these 5 neutral curves, either by movement of the maximum real part of the 5th curve into the unstable or stable half-plane ("co-periodic" stability, corresponding with super- or sub-criticality of the associated Hopf bifurcation), or by a "sideband" instability consisting of loss of tangency to the imaginary axis (first-order, or "hyperbolic" instability) or change in curvature (2nd order, or "parabolic" instability) of one of the 4 neutral curves through the origin; see Section 4.

For the quadratic nonlinearity, if $u(x)$ is a profile solution for a fixed β, then $-u(x)$ is a profile solution for $-\beta$, with the same value of ε. Thus, we are not able to produce a corresponding subcritical Hopf bifurcation by reversing the sign of β, but a mirror supercritical bifurcation.

To find examples of stable periodic profiles corresponding to both sub and supercritical Hopf bifurcations, we change the quadratic nonlinearity to a cubic nonlinearity in the next example, removing this symmetry and allowing us to change from super- to sub-by changing the sign of β.

5.3. Cubic nonlinearity

We consider next the system of conservation laws

$$u_t + A^\varepsilon u_x + N(u)_x = Du_{xx}, \tag{5.5}$$

with

$$A^\varepsilon := \begin{pmatrix} 1 & 0 & 0 \\ 0 & a_{22}^0 + \varepsilon & 0 \\ 0 & 0 & 3 \end{pmatrix}, \quad D := \begin{pmatrix} 1 & 0 & 2 \\ 0 & 1 & 1 \\ 1 & -2 & 1 \end{pmatrix}, \quad \text{and}$$
$$N(u) := \beta \begin{pmatrix} u_1^3 \\ 0 \\ 0 \end{pmatrix}, \tag{5.6}$$

where $a_{22}^0 = 2.605173614560316$. Similarly as the quadratic example, we vary ε as a bifurcation parameter. The stability of $u \equiv 0$ as ε varies is already shown in Figs. 1 and 2.

Starting from the supercritical periodic profile solutions found previously for the quadratic nonlinearity, we obtain a solution for the cubic nonlinearity by continuation in a homotopy variable $0 \le h \le 1$ via the nonlinearity $N(u) = [\beta(hu_1^3 + (1-h)u_1^2), 0, 0]^T$. To obtain a subcritical profile solution for the cubic nonlinearity, we use the approximate symmetry $(\beta, c, \varepsilon) \to (-\beta, -c, -\varepsilon)$, which is valid at the linear periodic level only. Thereafter, we solve for profiles using continuation.

In Fig. 4, we plot the bifurcating stable periodic solution through a supercritical Hopf bifurcation. Since $\varepsilon > 0$ for the constant solution to be unstable, as seen in Fig. 2, the periodic profile shown in Fig. 4(c) exists through a supercritical Hopf bifurcation. Fig. 4(b) shows the stable spectrum of the periodic profile shown in (c). Here

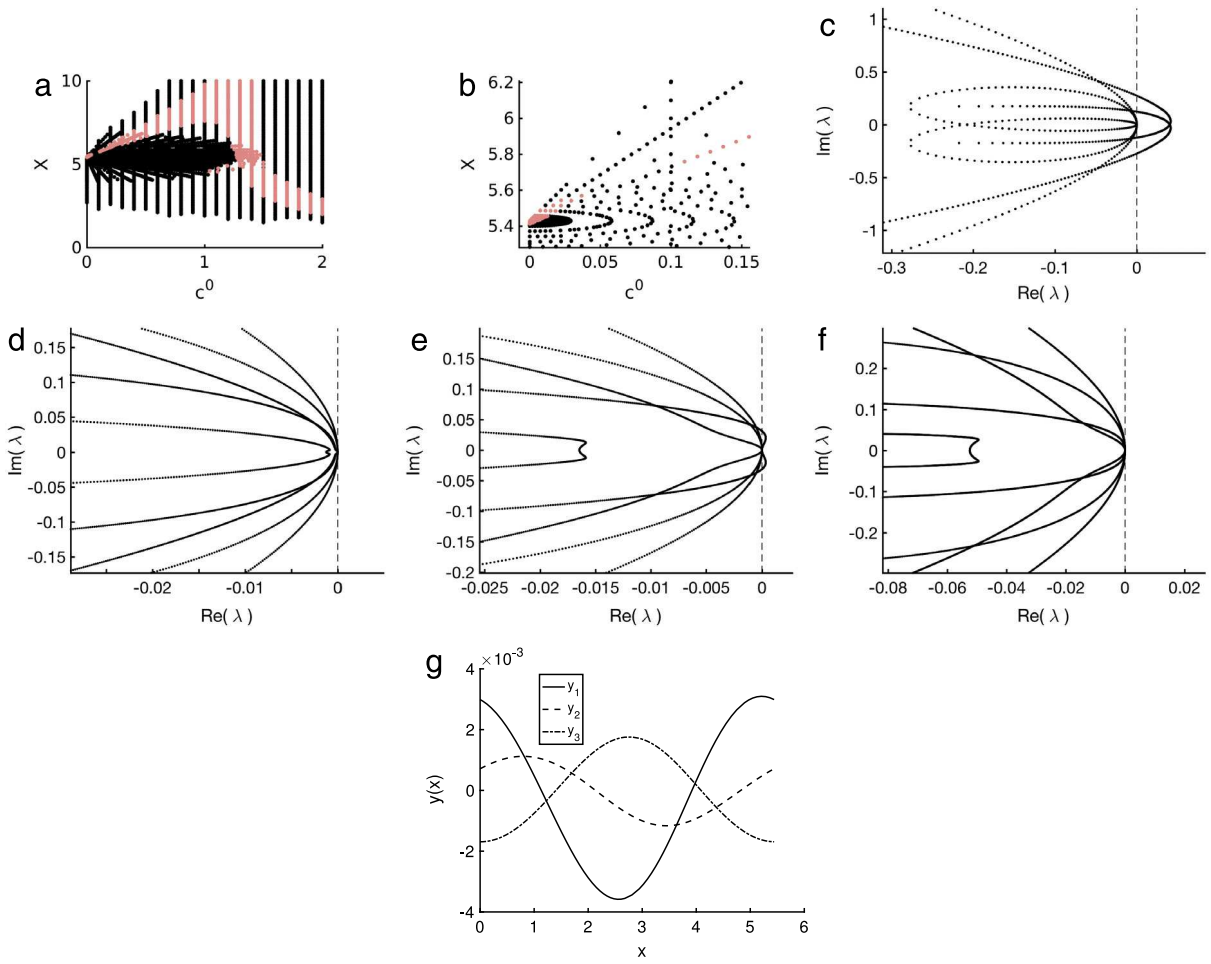

Fig. 3. (a) Stability bifurcation diagram in the coordinates of shifted wave speed $c^0 = c - c_*$ and period X. Pink dots (light dots in grayscale) and black dots correspond respectively to stable and unstable waves. (b) Zoom in of (a) showing a family of stable waves in parameter space leading to the point of the Turing bifurcation. There is a small region of instability separating the stable waves near the Turing bifurcation point and the large stability region. (c) Plot of the spectrum of the zero constant solution when $\varepsilon = 2.82e-3$, $c = c_* + 4.06e-3$, and $X = 5.44$, indicating that the Turing bifurcation corresponds to a supercritical Hopf bifurcation. (d) Plot of the spectrum of a periodic wave in the family of stable waves bifurcating from the Turing bifurcation. (e) Plot of the spectrum of a periodic wave in the family of unstable waves separating the two regions of stability. (f) Plot of the spectrum of a periodic wave in the large stability region. (g) Plot of the bifurcating periodic profile when $\varepsilon = 2.82e-3$, $c = c_* + 4.06e-3$, and $X = 5.44$, with component one marked with a solid line, component two with a dashed line, and component three with a dot-dashed line. Throughout $\beta = -10$ and a dashed line marks the imaginary axis.

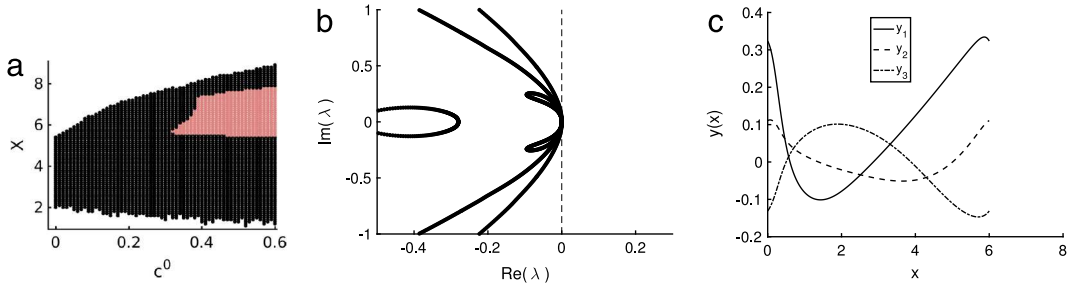

Fig. 4. (a) Stability diagram in the coordinates of shifted wave speed $c^0 = c - c_*$ and period X for $\beta = 10$. Pink dots (light dots in grayscale) and black dots correspond respectively to stable and unstable waves. (b) For a stable wave, we plot in (b) its spectrum and in (c) the wave itself, with $\beta = 10$, $c^0 = 0.5$, $X = 6$, and $\varepsilon = 8.74e-1$. A dashed line marks the imaginary axis in (b).

$\beta = 10$, $c^0 = 0.5$, $X = 6$, and $\varepsilon = 8.74e-1$. In Fig. 4(a), we plot a stability diagram in the coordinates of shifted wave speed $c^0 = c - c_*$ and period X. We do not find a family of stable waves bifurcating from the Turing instability.

By changing the sign of β, we find the stable periodic solutions through a subcritical Hopf bifurcation as demonstrated in Fig. 5. Since $\varepsilon < 0$ for the constant solution to be stable, as seen in Fig. 2, the periodic profile shown in Fig. 5(c) exists through a subcritical Hopf bifurcation. Fig. 5(b) shows the stable spectrum of the periodic profile shown in (c). Here $\beta = -10$, $c^0 = -0.3$, $X = 4.5$, and $\varepsilon = -3.5e-3$. In Fig. 5(a), we plot a stability diagram in the coordinates of shifted wave speed $c^0 = c - c_*$ and period X. We do not find a family of stable waves bifurcating from the Turing instability.

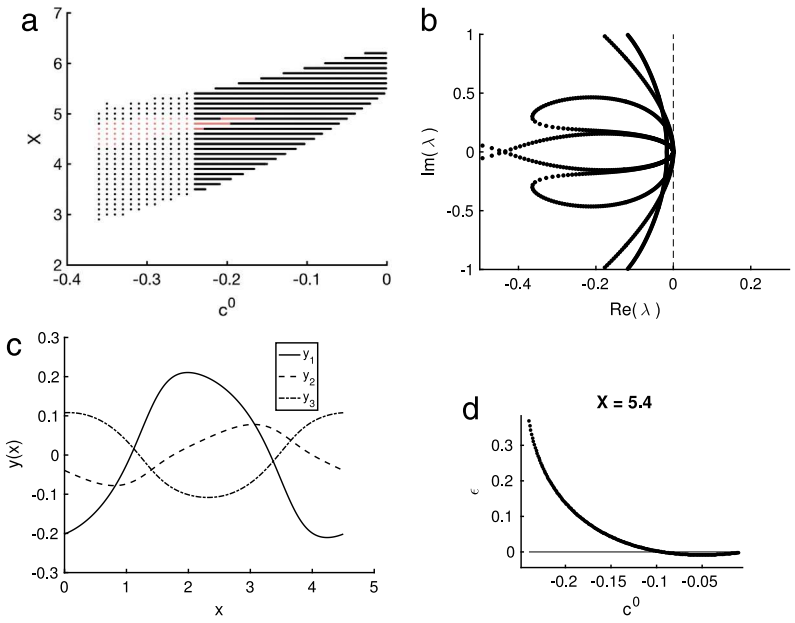

Fig. 5. (a) Stability diagram in the coordinates of shifted wave speed $c^0 = c - c_*$ and period X for $\beta = -10$. Pink dots (light dots in grayscale) and black dots correspond respectively to stable and unstable waves. For a stable wave, we plot in (b) its spectrum and in (c) the wave itself, with $\beta = -10$, $c^0 = -0.3$, $X = 4.5$, and $\varepsilon = -3.5e-3$. A dashed line marks the imaginary axis in (b). In (d) we plot a curve showing existence, up to numerical approximation, of periodic profiles of period $X = 5.4$ in the parameters c^0 and ε when $\beta = -10$ and the nonlinearity is cubic. A thin horizontal line marks the axis.

5.4. Numerical stability method

To determine the spectrum of the periodic profiles, we used Hill's method. The associated eigenvalue problem is given by $Lv = \lambda v$ where the linear operator L takes the form $L_{j,k} = \sum_{q=1}^{m_{jk}} f_{j,k,q}(x)\frac{\partial^q}{\partial x^q}$. The coefficients $f_{j,k,q}(x)$ are X periodic. As in [20], we use a Fourier series to represent the coefficient functions $f_{j,k,q}$, $f_{j,k,q}(x) = \sum_{j=-\infty}^{\infty}\hat{\phi}_{j,k,q}e^{i2\pi jx/X}$, and write the generalized eigenfunctions as $v(x) = e^{i\xi x}\sum_{j=-\infty}^{\infty}\hat{v}_j e^{i\pi jx/X}$, where $\xi \in (-\pi/2X, \pi/2X]$ is the Floquet exponent. Substituting these quantities into the eigenvalue problem and equating coefficients gives an infinite dimensional eigenvalue problem for each fixed ξ. By truncating the Fourier series at N terms and using MatLabs FFT function to determine the coefficients $\hat{\phi}_{j,k,q}$, we arrive at a finite dimensional eigenvalue problem $L_N^{\xi}\hat{v} = \lambda\hat{v}$, which we solve with MATLAB's eigenvalue solver. All computations were done using STABLAB [19]. For further information about Hill's method and its convergence properties, see [21–23].

5.5. Computational statistics

All computations were carried out on a Macbook pro quad core or a Leopard WS desktop with 10 cores. Computing a profile took approximately 2 s or less, and computing the spectrum via Hill's method took on average 20–60 s depending on the number of modes used. We typically used 101 Floquet parameters and 41 or 81 Fourier modes when using Hill's method. Each stability diagram took less then 24 h to compute on the Leopard WS desktop.

6. Discussion and open problems

We have identified an analog of Turing instability occurring for $n \times n$ systems of conservation laws of dimension $n \geq 3$, leading to a large family of spatially periodic traveling waves. Our numerical stability investigations give convincing numerical evidence that at least some of these waves are stable, answering the question posed in [1,6] whether there can exist stable periodic solutions of conservation laws.

Moreover, the same numerical investigations indicate that at least for some model parameters, the bifurcation diagram near Turing instability/Hopf bifurcation includes an open region of instability. This opens the possibility for rigorous proof of existence of stable periodic waves through a small-amplitude bifurcation analysis as carried out in [8–11] for the reaction–diffusion case. Such an analysis we consider an extremely interesting open problem. Note, however, that it is inherently more complicated than the reaction–diffusion version, involving $n+2$ bifurcation parameters (X, c, q), $X, c \in \mathbb{R}^1$, $q \in \mathbb{R}^n$ rather than the two parameters of the reaction–diffusion case. For an example of intermediate complexity, we point to the recent analyses [13,14] of reaction–diffusion equations with a single conserved quantity, featuring a three-parameter bifurcation.

Acknowledgments

Research of B.B. was partially supported under NSF Grant No. DMS-1400872. Research of S.J. was partially supported by the National Research Foundation of Korea(NRF) grant funded by the Korea government (MSIP) (No. 2016R1C1B1009978). Research of K.Z. was partially supported under NSF Grant Nos. DMS-0300487 and DMS-0801745.

References

[1] Myunghyun Oh, Kevin Zumbrun, Stability of periodic solutions of conservation laws with viscosity: Analysis of the Evans function, Arch. Ration. Mech. Anal. 166 (2) (2003) 99–166.
[2] Myunghyun Oh, Kevin Zumbrun, Stability of periodic solutions of conservation laws with viscosity: pointwise bounds on the Green function, Arch. Ration. Mech. Anal. 166 (2) (2003) 167–196.
[3] Denis Serre, Spectral stability of periodic solutions of viscous conservation laws: Large wavelength analysis, Comm. Partial Differential Equations 30 (1–2) (2005) 259–282.
[4] Mathew A. Johnson, Kevin Zumbrun, Nonlinear stability of periodic traveling waves of viscous conservation laws in the generic case, J. Differential Equations 249 (5) (2010) 1213–1240.
[5] Mathew A. Johnson, Pascal Noble, L. Miguel Rodrigues, Kevin Zumbrun, Nonlocalized modulation of periodic reaction diffusion waves: Nonlinear stability, Arch. Ration. Mech. Anal. 207 (2) (2012) 693–715.

[6] Alin Pogan, Arnd Scheel, Kevin Zumbrun, Quasi-gradient systems, modulational dichotomies, and stability of spatially periodic patterns, Differential Integral Equations 26 (3/4) (2013) 389–438.
[7] W. Eckhaus, Studies in Nonlinear Stability Theory, in: Springer tracts in Nat. Phil., vol. 6, 1965.
[8] A. Mielke, A new approach to sideband-instabilities using the principle of reduced instability, in: A. Doelman, A. van Harten (Eds.), Nonlinear Dynamics and Pattern Formation in the Natural Environment, in: Pitman Research Notes in Math, Longman, UK, 1995, pp. 206–222.
[9] Alexander Mielke, Instability and stability of rolls in the Swift-Hohenberg equation, Comm. Math. Phys. 189 (3) (1997) 829–853.
[10] G. Schneider, Diffusive stability of spatial periodic solutions of the Swift-Hohenberg equation, Comm. Math. Phys. 178 (3) (1996) 679–702.
[11] Alim Sukhtayev, Kevin Zumbrun, Soyeun Jung, Raghavendra Venkatraman, Diffusive stability of spatially periodic solutions of the Brusselator model. arXiv:1608.08476, (preprint), 2016.
[12] Blake Barker, Numerical proof of stability of roll waves in the small-amplitude limit for inclined thin film flow, J. Differential Equations 257 (8) (2014) 2950–2983.
[13] P.C. Matthews, S.M. Cox, Pattern formation with a conservation law, Nonlinearity 13 (4) (2000) 1293–1320.
[14] Alim Sukhtayev, Diffusive stability of spatially periodic patterns with a conservation law. arXiv:1610.05395, (preprint), 2016.
[15] Shuichi Kawashima, Systems of a Hyperbolic-Parabolic Composite Type, with Applications To the Equations of Magnetohydrodynamics (Ph.D. thesis), Kyoto University, 1983.
[16] A.M. Turing, The chemical basis of morphogenesis, Philos. Trans. R. Soc. B 237 (641) (1952) 37–72.
[17] Myunghyun Oh, Kevin Zumbrun, Low-frequency stability analysis of periodic traveling-wave solutions of viscous conservation laws in several dimensions, Z. Anal. Ihre Anwend. 25 (121) (2006).
[18] Mathew A. Johnson, Pascal Noble, L. Miguel Rodriguez, Kevin Zumbrun, Behaviour of periodic solutions of viscous conservation laws under localized and nonlocalized perturbations, Invent. Math. 197 (1) (2014) 115–213.
[19] Blake Barker, Jeffrey Humpherys, Joshua Lytle, Kevin Zumbrun, STABLAB: A MATLAB-based numerical library for evans function computation. https://github.com/nonlinear-waves/stablab.git.
[20] Bernard Deconinck, Firat Kiyak, John D. Carter, J. Nathan Kutz, SpectrUW: A laboratory for the numerical exploration of spectra of linear operators, Math. Comput. Simulation 74 (4–5) (2007) 370–378.
[21] Christopher W. Curtis, Bernard Deconinck, On the convergence of Hill's method, Math. Comp. 79 (269) (2010) 169–187.
[22] Bernard Deconinck, J. Nathan Kutz, Computing spectra of linear operators using the Floquet–Fourier–Hill method, J. Comput. Phys. 219 (1) (2006) 296–321.
[23] Mathew A. Johnson, Kevin Zumbrun, Convergence of Hill's method for nonselfadjoint operators, SIAM J. Numer. Anal. 50 (1) (2012) 64–78.